Main Challenges for High Performance NAS Battery: Materials and Interfaces

Zhaoyin Wen, Yingying Hu, Xiangwei Wu, Jinduo Han, and Zhonghua Gu*

The progress in the research work and real applications of sodium-sulfur (NAS) battery in large scale energy storage is introduced. The key materials and interfaces of the battery, particularly the role of Shanghai Institute of Ceramics, Chinese Academy of Sciences (SICCAS), are systematically reviewed. As the most important and difficult part, the high-quality beta-alumina ceramic electrolyte tubes are prepared by a low-cost solid state reaction process; their sealing performance and interfacial behavior with molten sodium and sulfur electrodes could be substantially improved by glass ceramic type sealants and surface modification, respectively. Combination of carbon and additives like SiO_2 with different wetting behaviors for sulfur and the discharge product sulfides is shown to be significant in improving the electrochemical performances of NAS battery. Conductive ceramic coatings are developed as anti-corrosion media of the current collector of sulfur electrode; this is identified as an effective route to protect the metal parts.

1. Introduction

In recent years, world-wide renewable energy research has been focused heavily on large capacity energy storage, so that clean energy sources like solar and wind power which are by nature unpredictable and greatly dependent on weather, can be ultimately utilized.[1] In addition, load leveling of electricity grid by large-scale energy storage is in more and more urgent demand, especially for cities and even countryside, due to the growing economic and social development. Many kinds of physical and chemical energy storage technologies have been developed recently. For such purposes, several criteria must be considered, including lifetime, life cycle, power and energy, self-discharge rates, environmental impact, cycle efficiency, capital cost, storage duration and technical maturity. Among all chemical energy storage technologies, the medium-temperature rechargeable sodium-sulfur batteries, although they were originally developed by Ford in the late 1960s and 1970s for electrical vehicle applications, are well-suited for stationary energy storage for the electrical grid owing to their high theoretical specific energy (~760Wh kg^{-1}), high energy efficiency, cycling flexibility, high rate pulse power capability, and low maintenance requirements.[1–4] Moreover, NAS batteries are environmentally benign, since the batteries are sealed and thus allow no emissions during operation. More than 99% of the overall weight of the battery materials can be recycled. Only sodium must be handled as a hazardous material.

After several decades of research and development, NAS battery technology has been demonstrated on the grid in Japan and other countries, where it is largely used in utility-based load-leveling and peak shaving applications. In the last decade, NAS battery-based installations have grown exponentially from 10 MW in 1998 to 300 MW/2000 MWh in April 2009, and to over 350 MW by the year 2010. The production capacity of NGK Insulators Inc. has reached 150 MW per year and there are plans to ramp up the annual production capacity to 210 MW in 2011.[5] More than 250 locations with power larger than 500 KW are built by NGK and are operating in Japan and other countries. A 34 MW/245 MWh system was installed in northern Japan for stabilizing a 51 MW wind farm, and it is the largest energy storage system in the world, apart from pumped hydroelectric storage (PHS) and compressed air energy storage (CAES) systems.[6] It is claimed that NAS battery is the most economically feasible battery storage option for energy management, requiring electricity prices of 32 cents/kW h.[4]

Recently, the NAS technology and other beta-alumina ceramic electrolyte based batteries have also been recently promoted in other countries including USA, China, Korea, Switzerland, etc. In China, the research work on NAS batteries for EV application dates back to late 1960's. The work on NAS battery research for large scale energy storage applications started in 2006 with the collaboration of the Shanghai Electric Power Company. A 2 MW pilot production line for 650Ah single cells was constructed, thereafter a 100 MW/800 MWh energy storage system was demonstrated since the 2010 Shanghai World Expo. A mass production company was established recently with joint investment of the Shanghai Electric Group and the Shanghai Electric Power Company.[7]

Although the application scale of the NGK NAS batteries expanded year by year and especially increased sharply in the last 3–5 years, the large-scale commercialization of NAS batteries still demands better performances, safety improvements, and level of automation in the fabrication of high-quality

Prof. Z. Wen, Dr. Y. Hu, Prof. X. Wu, Prof. J. Han, Prof. Z. Gu
CAS Key Laboratory of Materials for Energy Conversion
Shanghai Institute of Ceramics
Chinese Academy of Sciences (SICCAS)
Shanghai 200050, China
E-mail: zywen@mail.sic.ac.cn

DOI: 10.1002/adfm.201200473

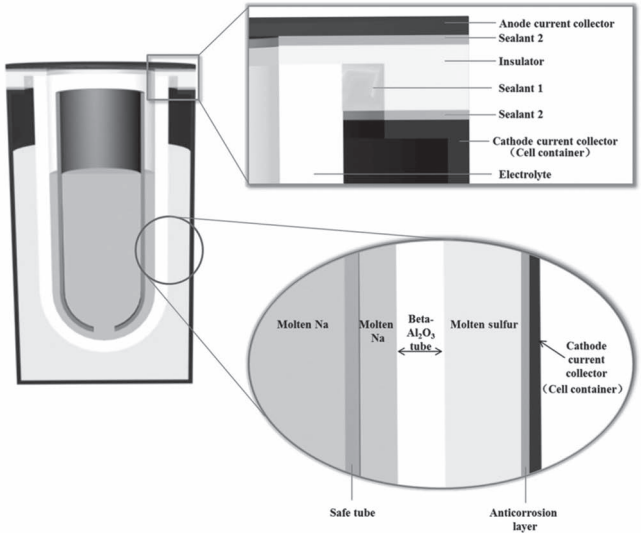

Figure 1. Schematic illustration of a tubular designed NAS cell.

ceramics for cost reduction, which depends on the development of new functional materials and novel cell designs.[8,9]

NAS batteries are commonly constructed in tubular designs, as schematically shown in **Figure 1**. As indicated, the battery is basically composed of a beta-alumina ceramic tube acting simultaneously as a solid electrolyte and a separator, sodium anode and sulfur cathode, which are assembled with current collectors and insulators. NAS batteries typically operate at temperatures between 300 and 350 °C to keep the electrode materials in a molten state, and convert electrical energy to chemical potential via the following reactions:[10]

$$Anode:\ 2Na - 2e^- \leftrightarrow 2Na^+ \quad (1)$$

$$Cathode:\ xS + 2Na^+ + 2e^- \leftrightarrow Na_2S_x\,(x = 3 \sim 5) \quad (2)$$

$$Cell\ Reaction:\ 2Na + xS \leftrightarrow Na_2S_x\,(x = 3 \sim 5) \quad (3)$$

The working voltage of NAS batteries is in the range of 1.78–2.076 V at 350 °C.

The solid state electrolyte, usually beta-alumina ceramic tube, is acknowledged to be the key element for determining battery operation and cost.[11] In addition, for both safety and performance reasons, the sealing of all the parts of NAS battery must be of high-integrity and gastight, the sealants and current collectors are also important materials to be considered with highly stable properties since they faced to the active and corrosive electrode materials. This paper reviews the available literatures on the key materials and interfaces in NAS batteries; especially highlighting our recent relative research progress.

2. β″-Alumina Ceramic Electrolyte

2.1. Structural Feature

β″-alumina is the preferred electrolyte system applied in NAS battery, acting as the electrolyte and the separator, and belongs to the beta-alumina subgroup of sodium aluminates with layer type structure.[11] As **Figure 2** illustrates, β″-alumina is composed of closely packed spinel type blocks, referred to as spinel blocks, separated by loosely packed slabs containing mobile sodium ions which are free to move under an electric field. Each closely packed block has four layers of oxygen ions with aluminum ions in both octahedral and tetrahedral interstices and bonded together by the sodium ions and Al-O-Al bonds in the interlay.[12] The typical ionic conductivity of β″-alumina is as high as 0.2–0.4 Scm^{-1} at 300 °C, which can be an excellent electrolyte for sodium batteries.[13,14] However, β″-alumina crystals lack stability, thus Li^+ and Mg^{2+} are the most popular doping ions to stabilize the β″-alumina with the ideal compositions of $Na_{1.67}Al_{10.33}Mg_{0.67}O_{17}$ and $Na_{1.67}Al_{10.67}Li_{0.33}O_{17}$, respectively.[15]

It is noticeable that various kinds of defects possibly exist in β″-alumina. They remarkably affect the overall properties of NAS batteries. The defects can resulte from composition deviation, impurity phase and grain boundary, crystal intergrowth, dislocation, etc. Composition design and precise control for the whole material processes are critical to guarantee the quality of the β″-alumina electrolyte.

2.2. Powder Synthesis

Significant work has been done to synthesize β″-alumina powders by various processes such as conventional solid-state calcination, sol-gel route, co-precipitation technique, spray-freeze/freeze-drying method, mechanochemical processing, etc.[11–13,16–20] Usually, the synthesis temperature for solid-state reaction is above 1600 °C; sodium loss and exaggerated grain growth are inevitable during the high temperature heating process, which results in the mixture of β- and β″-alumina with lower conductivity and duplex microstructure with large grains in a fine-grained matrix.[17] For the purpose of optimizing the solid-state approach, Vanzyl et al. obtained pure β″-alumina at the temperature as low as 1200 °C, using hydroxyl alumina group, such as boehmite and bayerite as the starting precursors.[21,22] Compared to the solid-state reaction process, the solution-based chemical methods decrease the synthesis temperature and can

Professor Zhaoyin Wen obtained his BA in Materials Science in 1984 from the Nanjing University of Chemical Technology, China, M.S. degree and Ph.D. from the SICCAS in 1987 and 1998, respectively. He was a post-doctoral researcher in Mie University, Japan, during 1999 to 2001. He has been working in SICCAS since 1987. Currently, his research interests include fundamental and application researches of fast-ion conductors, secondary batteries like sodium sulfur battery, lithium sulfur battery, lithium air battery, etc.

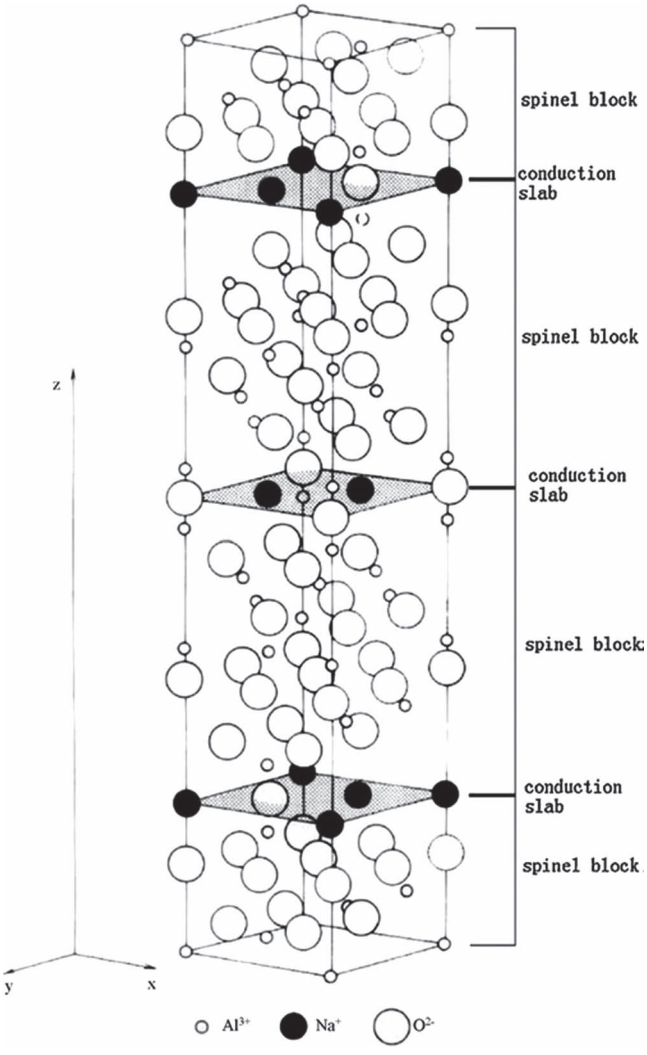

Figure 2. Perspective drawing of the idealized structure of β″-alumina. Reproduced with permission.[26] Copyright 2008, Elsevier.

produce powders with more homogeneous microstructure and higher sinterability. However, β-alumina cannot be eliminated completely from the final products via these processes.[23,24]

In order to realize the homogenization of the small amount of the lithium content in β″-alumina powders and the final ceramic products, a double-zeta powder process was established by this lab in 1980's.[25] The powder process employed the synthesized zeta-lithium aluminate ($Li_2O \cdot 5Al_2O_3$) and zeta-sodium aluminate ($Na_2O \cdot 5Al_2O_3$) (both at 1250 °C) as precursors for the β″-alumina powders. The experimental results indicated that the double-zeta method together with spray drying produced more homogeneous powders than normal solid state reaction because of the pre-dilution for the minor component lithium in the major component alumina.[26,27]

2.3. Ceramic Tube Fabrication

As the solid electrolytes and separator in a practical sodium battery, β″-alumina is usually designed in one-end closed tubular form.[28] The β″-alumina tube electrolyte should meet the following requirements to confirm the high quality of NAS battery: (1) high sodium ion conductivity, (2) low electronic transference number, (3) high relative density, (4) high mechanical strength and (5) long-term durability against corrosion.[27] Fabrication of β″-alumina ceramic tube with a dense and fine-grained microstructure is rather difficult. Isostatic pressing, electrophoretic deposition, extrusion techniques, etc., have been developed to prepare the β″-alumina tubes.[12,15,29–31] In an electrophoretic deposition, β″-alumina powders are dispersed in an organic dielectric liquid in which a mandrel is placed. Then an electrical field is applied between the mandrel and a counter electrode and powders are deposited evenly onto the mandrel. The technique produces uniform green tubes but removal from the mandrel is difficult. Extrusion is an economically attractive way of making tubes but lacks a suitable binder system due to the strong basicity of β″-alumina.[29] Isostatic pressing is a relatively simple, low cost and high efficiency method, and is the most commonly used technique to form β″-alumina green tubes. Isostatic pressing has many advantages, for example binder as low as 1–2 wt% added to the precursor powders to be formed, high green body strength for handling and post cutting to a designed length, and high efficiency with readily raised production rates.

Isostatic pressing based on a double-zeta powder process is carried out to fabricate β″-alumina ceramic tubes in this lab.[26,27] Powders with high fluidity are obtained by slurry spray drying process, which are necessary to guarantee the quality of the green tubes.

Figure 3 demonstrates the good fluidity of the powders. As shown, the spray-dried powders possess an average size of 50 μm. **Figure 4** illustrates β″-alumina ceramic tubes with different sizes prepared in SICCAS, together shown as the insets are the typical microstructure and cross section image of the tube. As shown , the ceramic tubes display good circularity without obvious deformation. **Table 1** lists the basic properties of the ceramic tubes prepared in SICCAS.[26] Sintering is the most difficult process to control and potentially the most expensive operation involved in the preparation of β″-alumina ceramic tubes. It usually takes place with the assistance of liquid phases which easily result in deformation of the final ceramic tubes. The densification of the ceramics

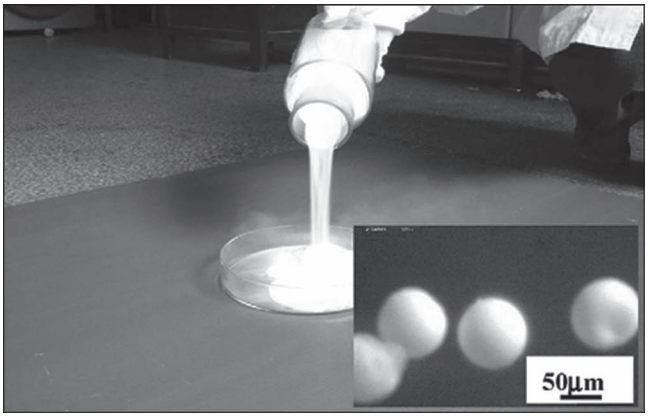

Figure 3. Precursor powders with good fluidity and spherical particle morphology. Reproduced with permission.[26] Copyright 2008, Elsevier.

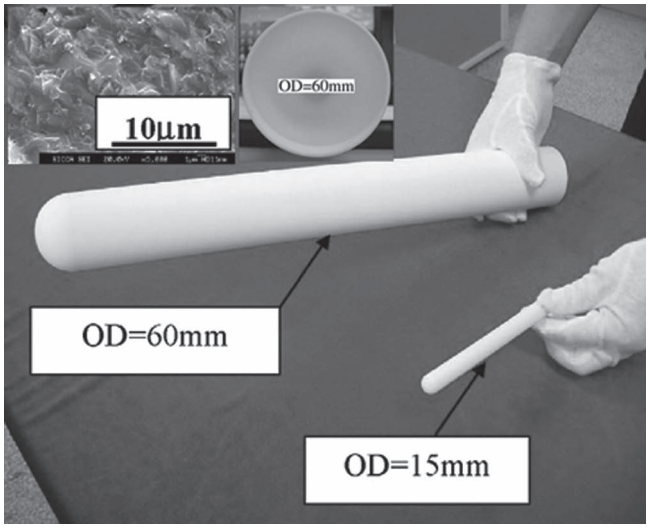

Figure 4. Beta-alumina ceramic tubes of different outer diameters prepared in SICCAS. Reproduced with permission.[26] Copyright 2008, Elsevier.

Table 1. Properties of β''-alumina ceramic tubes prepared by SICCAS.

Property	Value
Outer diameter (mm)	10–60
Length (mm)	100–600
Thickness (mm)	1.0–1.5
Chemical composition (wt%)	Na_2O: 9.0, Li_2O: 0.72, Al_2O_3: balance
Relative density (%)	99
Relative β''-alumina phase content (%)	99
Matrix grain size (μm)	1–5
Sodium ion resistivity at 300 °C (Ωm)	4-6
Bending strength (MPa)	250 ± 26

proceeds in parallel with phase transformation to β''-alumina and grain growth. Loss of the volatile alkaline elements, especially deformation decrease in circularity, and the exaggerated grain growth of the ceramics are the main factors to be preferably considered. Both vertical and horizontal batch sintering processes were developed in SICCAS, by which high-quality ceramic tubes were fabricated.

Table 2. Properties of β''-alumina ceramic tubes prepared by SICCAS.

ZrO_2 in composite (vol.%)	Y_2O_3 in ZrO_2 (mol.%)	Bending strength (MPa)	Fracture toughness (MPa $cm^{1/2}$)	Resistivity at 300 °C (Ω cm)
0	/	250	2.3	5.7
10	2.5	278	3.1	9.3
15	2.5	314	3.4	9.8
20	2.5	330	3.7	11.0
15	6	270	3.0	9.8

2.4. Composite and Mechanical Properties

The mechanical properties of β''-alumina depend mainly on the relative density and microstructure of the ceramic electrolyte.[10] Dense β''-alumina ceramics with fine grains exhibit much higher fracture strength.[32,33] The defects such as cracks and impurities also influence the mechanical strength significantly. The transformation from tetragonal-ZrO_2 (t-ZrO_2) to monoclinic-ZrO_2 (m-ZrO_2) has been used successfully to toughen and strengthen many ceramic systems. It was also employed to β''-alumina by many laboratories.[34–37] Improvement of the mechanical strength and K_{IC} (the fracture toughness) of the β''-alumina ceramics should lead to significant enhancement of the battery life. **Table 2** summarizes the mechanical and electrical properties of typical β''-alumina/ZrO_2 composites.[26] As observed, the strengthening and toughening effect of ZrO_2 is significant, while the electrical properties is comparable to that of the pristine β''-alumina at the amounts of ZrO_2 not more than 15 vol.%.

The strengthening effects of ZrO_2 addition may result from several mechanisms, including transformation toughening, deflection toughening and microstructure optimization.[17] The effect in the t-ZrO_2 containing composite is even more remarkable than the c-ZrO_2 containing composite. Moreover, microcrack toughening and crack deflection mechanisms are mainly attributed to the c-ZrO_2 containing composite. The t-m phase transformation mechanism is ascribed to the main toughening and strengthening effects of the t-ZrO_2-based composites.

3. Sealing Materials

NAS battery operates at a temperature above 300 °C in order to keep the discharge products in the liquid state and improve the cell performance. Sodium and sulfur are also in melting state at the operating temperature. If the melts of both electrodes are in direct contact with each other, the reactions between them are inherently violent, potentially leading to fire and even explosion.[7] It is easy to see from Figure 1 that the breakdown of any parts in the NAS cell facing both Na and S electrode would cause the direct contact of the electrodes. Such parts include the β''-alumina ceramic electrolyte tube, the insulator, α-alumina, the sealant 1 connecting the electrolyte and the insulator, as well as the sealant 2 connecting the insulator and the current collectors. Among all the parts, the sealant 1, normally a glassy material, is the weakest one. Borosilicate glass has usually been selected due to its high mechanical strength and chemical durability.[15] However, the glass sealants have inherent disadvantages like high brittleness, high sealing temperature, easy cristobalite precipitation, and poor thermal expansion match with the sealed parts.[38] The seal creates a major challenge in the development of NAS battery. However, few works about glass sealants for NAS battery were reported except for some patents.[39–42] The data in these patents are not systematically and completely opened. In recent years, new types of sealants, such as glass-ceramics, Bi-doped borosilicate glass

Table 3. TECs of the sealants obtained at different conditions.

Y_2O_3 contents (wt.%)	Thermal treatment	TECs ($\times 10^{-6}$ K^{-1})	
		25–300 °C	25–400 °C
G1: 0.5	1000 °C × 7 min	6.5	6.7
G2: 1.0	1000 °C × 7 min	6.3	6.5
G3: 3.0	1000 °C × 7 min	5.1	5.7
3.0	1000 °C × 7 min, 800 °C × 90 min	6.9	6.4
3.0	1000 °C × 7 min, 700 °C × 120 min, 800 °C × 90 min	6.6	6.5

have been developed in SICCAS and exhibit superior thermal expansion match and chemical compatibility.[38,43–46]

3.1. Glass-Ceramic Sealants

Compared to commercial borosilicate glass sealants, glass-ceramic sealants possess several advantages: (1) high strength; (2) high chemical stability; (3) no phase transformation and ignorable stress during thermal cycles and (4) controllable thermal expansion. Borosilicate glass was chosen as the basic glass and TiO_2 as the nucleating agent. Large radii and high field intensity Y_2O_3 was doped to modulate the thermal expansion coefficient (TEC) and CaF_2 was further added to decrease the viscosity of the borosilicate glass.

The effects of Y_2O_3 contents and the thermal treatment process on the TECs of the glass-ceramic sealants were investigated. **Table 3** lists the TECs of the sealants obtained at different conditions.[44] As observed, at Y_2O_3 doping level of 0.5, 1.0, 3.0 wt.%, the TECs of the glass-ceramic sealants were well-matched with those of the α-alumina and β''-alumina, which were 6.9×10^{-6} K^{-1} and 6.6×10^{-6} K^{-1} from room temperature to 300 °C, respectively. The TECs of the sealants at Y_2O_3 dopant of 0.5 and 1.0 wt.% were adaptive while sealed at 1000 °C for 7 min. However, when the doping level is increased to 3.0 wt.%, the sealant should be heated at 800 °C for 90 min to realize a satisfactory TEC match.

The glass-ceramic sealants displayed favorable performance. Even after 100 times thermal shock, the interfaces between the 3.0% Y_2O_3 doped glass-ceramics and α-alumina or β''-alumina were still kept intact and highly bonded, as shown in **Figure 5**a and b. The thickness of the diffusion layer was less than 10 μm after heat treating at 350 °C for 850 h, indicating favorable chemical match of the sealants with alumina. However, a few pores were found in the sealants, which resulted from the glass crystallization at the sealing temperature. Replacing part of SiO_2 in the glass by Bi_2O_3 can depress the precipitation of cristobalite effectively and realize densification of the glass-ceramic sealants.[38]

3.2. Bi-Doped Borosilicate Glass

Substituting Bi_2O_3 for part of SiO_2 in borosilicate improved the thermal expansion match between the glasses and α-alumina

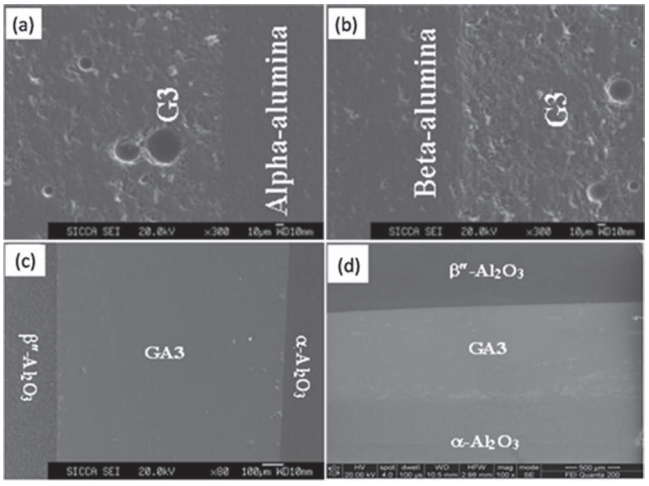

Figure 5. (a, b) Cross-sectional images of the α-alumina/3.0% Y_2O_3 doped glass-ceramic (G3) sealant/β''-alumina interfaces after thermal shock for 100 times. Reproduced with permission.[44] Copyright 2010, Springer. Cross-sectional morphologies of β''-alumina/glass sealant with Bi_2O_3 dopant of 32wt.% (GA3)/α-alumina interfaces heat-treated at 800 °C for 7 min (c) before thermal shock and (d) after thermal shock for 200 times. Reproduced with permission.[45] Copyright 2011, Elsevier.

or β''-alumina. The glass transition temperature (*Tg*), the softening temperature (*Ts*) and the viscosity of the doped glass were decreased. It was assumed that the replacement of SiO_2 by Bi_2O_3 made the glass network less rigid and Bi_2O_3 built the glass network as [BiO_6] unit, which gave rise to the decrease in the viscosity. A viscosity about 10^5 Pa s was achieved at 800–850 °C, making the sealing temperature 200 °C lower than that of the undoped one.[38]

The density of Bi-doped glass sealants was elevated obviously due to the optimized viscosity.[46] Figure 5c illustrates the cross-section morphologies of the interfaces between α-, β''-alumina and the glass sealant with Bi_2O_3 dopant of 32wt.% (GA3 glass). As seen, the β''-alumina/GA3 glass/α-alumina interfaces were joined well without any microcracks and the joint was pore free and indicated perfect hermeticity. The bonding strength reached as high as 17.91 MPa. After 200 times thermal shock, no obvious changes were found except the formation of a thin diffusion layer between the GA3 glass and β''-alumina (Figure 5d). After thermal shock, Al diffusion from β''-alumina to GA3 glass produced the diffusion layer with thickness of about 7 μm and no diffusion of Si, Bi, Na occurred from glass into α-, β''-alumina. The 7 μm diffusion layer could be ignored compared with the electrode operation area, which would present little influence on the performance of the electrolyte materials.

4. Sulfur Electrode

In a practical NAS battery, the constituents of the sulfur electrode include the sulfur that is reduced during discharge and the graphite or carbon felts that are commonly used as the electronically conductive matrix material.[15,47] During the first ten years (1968–1977), the cells were filled with molten sulfur after the graphite or carbon felt had been packed into the cells. This

technique presents several disadvantages such as long calcination duration, large structural and compositional inhomogeneity, high resistance, complex synthesis route etc.

The sulfur electrode manufacture now widely used by the developers was preformed sulfur electrode technique, which was first described by Storey's patent.[48] In this technique, the electrodes are made up from elements which are shaped in a mould under compression whilst impregnated with liquid sulfur. While the felt is still under compression the sulfur is cooled and solidified. These solid preforms are inserted into cells during assembly, and when the cell is heated up the sulfur melts and allows the graphite or carbon matrix to expand and contact the collector and the beta-alumina ceramic surfaces. The advantages of this method were ease of cell assembly, rapid production, low resistance and a less uneven loading of felt into the cathode compartment.[15]

To obtain the sulfur electrode with good performance, not only a low cathode resistance is required, but it is preferable to make the fibers parallel to current flow. Thus two different electrode structures have been developed.[47] The purpose of both methods is to reduce the amount of elemental sulfur that forms on the electrolyte surface during recharge, which will be discussed carefully in the Interface subsection. One method uses physical components that are preferentially wet by sodium polysulfides[49] and the other alters the electric-potential distribution in the sulfur electrode by using graded-porosity carbon or graphite felt. In general, the first method produces cells with better recharge characteristics. However, this method can be more costly because of the complicated structure.

In our lab, we have studied the influence of heat treatment of carbon felt on the performance of the sulfur electrode. **Figure 6** shows the morphology of carbon felt heat-treated at 550 °C. Abundant nanoscale pores formed on the surface of carbon felt after heat treatment, which was of benefit to the absorption of the electrode materials. As displayed in **Figure 7**, the electrical conductivity of the carbon felt increased with the increase of heat-treatment temperature, and it reached a maximum for the sample treated at 550 °C. Further increase of the treating temprature caused decrease in conductivity.

In addition, we have designed a carbon felt with SiO_2 fibers punched, as shown in **Figure 8**. It was found that the C/SiO_2 composite show remarkably improved electrochemical behavior as demonstrated in **Figure 9**, the cycling stability of the NAS cell was improved significantly with the additive, and the over-

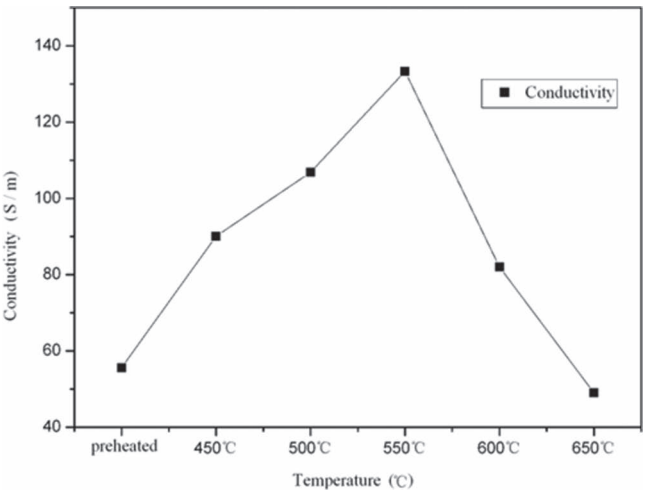

Figure 7. Electrical conductivity of carbon felt after heat-treated at different temperatures.

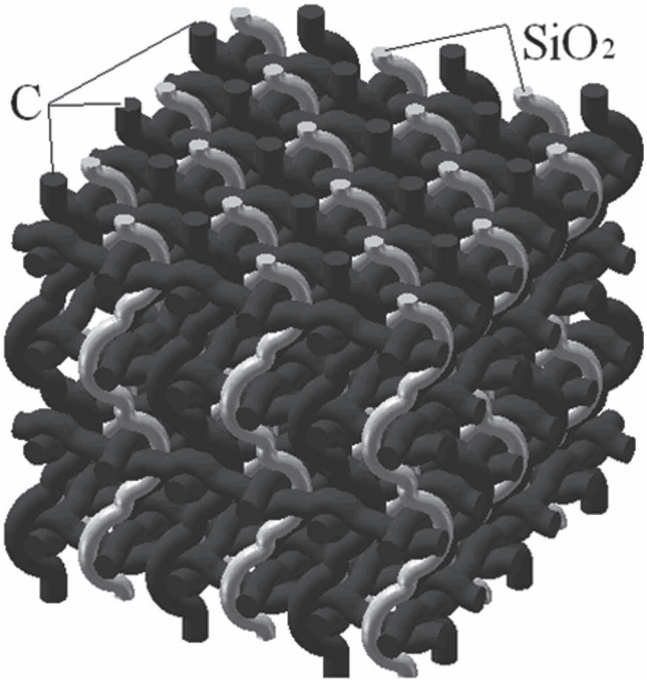

Figure 8. The structure of the C/SiO_2 composite felt.

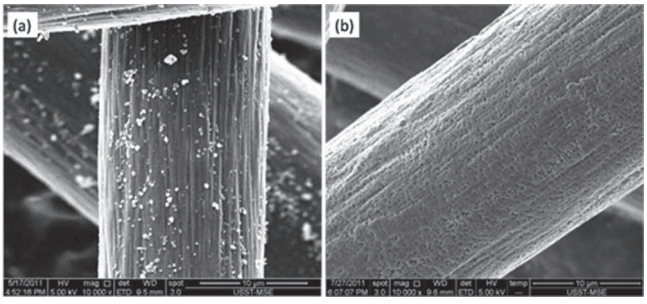

Figure 6. SEM images of carbon felt before and after heat-treated at 550 °C.

potential of the NAS cell greatly decreased with the SiO_2 additives. The addition of 35wt% SiO_2 showed further improvement in the charge and discharge behavior as shown in **Figure 10**. Moreover, The 35wt% SiO_2 containing composite carbon felt showed better cycling stability that the 20wt% SiO_2 based cell. The improved performance of the C/SiO_2 composite felt was supposed to be connected with the different absorbing and wetting performance of the carbon and the SiO_2 surfaces, which caused selective absorption of the sulfur and the resulted sodium sulfide between the C and the SiO_2 surfaces, giving an abundant reactive region for the cell reactions, as schematically illustrated in **Figure 11**.

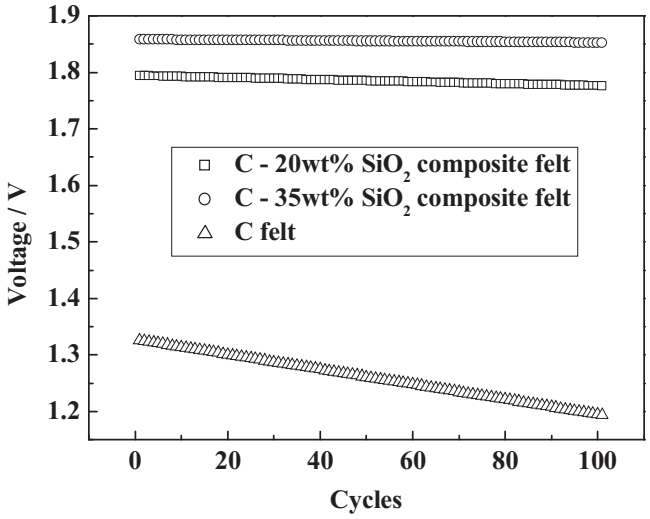

Figure 9. The cycling stability of NAS battery with different carbon fibres in sulfur electrode.

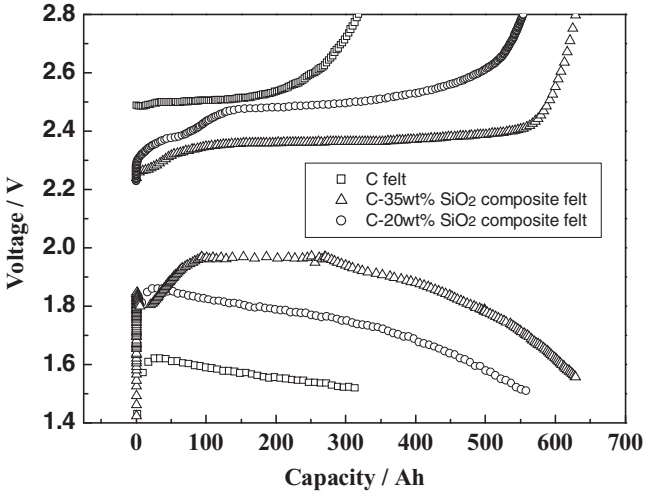

Figure 10. Charge and discharge profiles of Na-S battery with different carbon fibres in sulfur electrode.

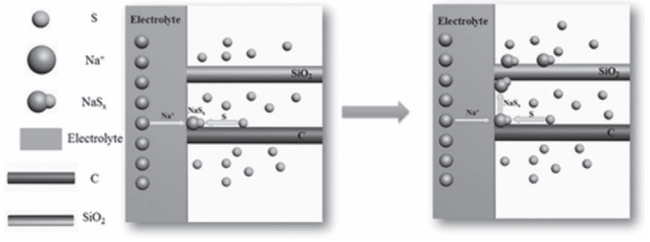

Figure 11. Illustration of the formation and transport of the sodium sulfide in the sulfur electrode with composite backbone.

5. Interface and Surface Modification

The cell reactions take place at the interfaces of β''-alumina and sodium electrode or sulfur electrode respectively. The interface behavior of the cell is one of the key factors determining the cell electrochemical performances. Hence, the interfaces between the liquid electrodes and β''-alumina electrolyte have been considered to be crucial for the development of a satisfactory NAS cell.

5.1. Sodium/β''-Alumina Interfacial Polarization

In order to ensure that the sodium electrode does not considerably contribute to the cell resistance, the Na/β''-alumina interfacial polarization has to be kept to a minimum, and the sodium anode has to be maintained in contact with the full area of the β''-alumina surface during the cell operation life.

It was expected that liquid sodium would be an ideal reversible electrode and the polarization problems would not arise from the Na/β''-alumina interface. However, a mass of polarization has been observed at the interface during the past decades. Sudworth et al. have investigated the AC resistance and DC cyclic galvodynamic polarization curves of the Na/β''-alumina interface via a tubular Na/β''-alumina/Na system in 1973.[50] The AC resistances of the symmetrical cell decreased as the frequency increased. The non-ohmic, asymmetric, and sweep rate-dependent behavior of the polarization curves were illustrated at all temperatures. In addition, the contrast experiments in this work demonstrated that the oxide content of the sodium was not the reason for the appearance of the polarization, instead the polarization was more severe when the sodium has a lower degree of purity. This is consistent with the observations of Bradhurst and Buchanan.[51] Their work indicated that dissolved oxide could enhance the wetting of ceramics. The polarization might be attributable to the incomplete wetting of the β''-alumina by sodium.

It is worth mentioning that attempts to measure the Na/β''-alumina interfacial resistance directly from the AC impedance spectra of the planar Na/β''-alumina/Na cell at temperatures between 150 and 350 °C have been conducted by Armstrong and his coworkers.[52] **Figure 12** a presents the complex impedance of polished β''-alumina surface at 150 °C. As proposed in this work, based on the fitted equivalent electrical circuit shown in Figure 12b, the impedance spectrum displays an intercept R_∞

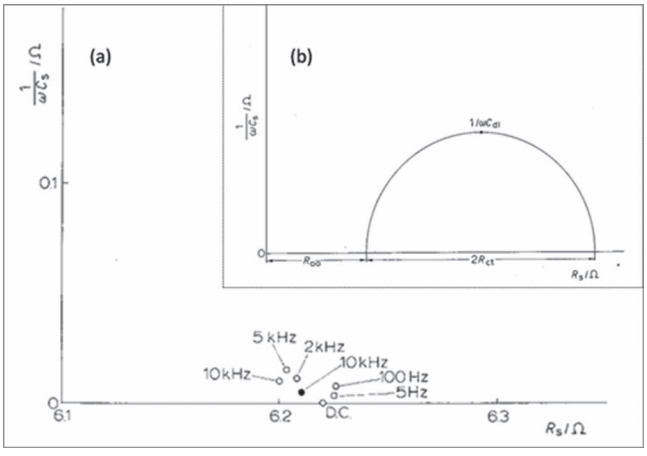

Figure 12. a) The complex impedance of polished β''-alumina surface at 150 °C. b) The proposed corresponding fitted equivalent electrical circuit.[52]

on the real axis, corresponding to the resistance of the β''-Al_2O_3 (including the bulk resistance and grain boundary resistance), and a semi-circle at lower frequencies derive from the interfacial resistance (mainly charge-transfer resistance R_{ct}). The article pointed out that both the polished and rough β''-alumina surface introduced a certain amount of R_{ct}, but the enhanced wetting of the surfaces by sodium conduced to the decrease of the interfacial resistance. Later, more work on the impedance of the β''-alumina and sodium-based substance interface have been employed to discuss the transfer of Na^+ across the interface and the influence factor (for example water vapour) of the interfacial resistance.[53–60]

Besides the viewpoints concentrating on the incomplete wetting of the electrolyte surface, Breiter et al. who used other three testing systems to study the behavior of different sodium electrode/β''-alumina interface reported that the asymmetric behavior involved a larger effective resistance during anodic sodium dissolution than during cathodic sodium deposition, suggesting that a thin passivating Na_2O film formed on the interface during the sweep caused the polarization.[61] The voltammetric current–potential curves for the cell Cu/Al/Na/β''-alumina/$NaNO_3$/Pt/Cu shown in **Figure 13**. The asymmetric curve shape showed a strong sweep rate dependence. Like the above-mentioned point of view, they attributed the asymmetry to the effects of the sodium/β''-alumina interface, but there is no further explanation for how the passivating film acts in the cycling process.[61,62]

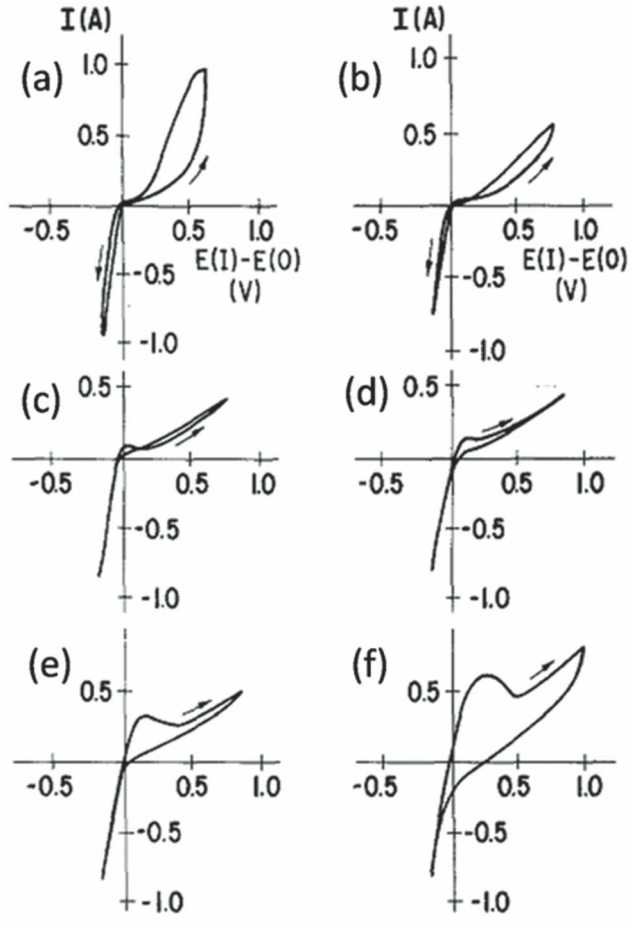

Figure 13. The voltammetric current–potential curves for the cell Cu/Al/Na/β''-alumina/$NaNO_3$/Pt/Cu. a) 0.001, b) 0.01, c) 0.1, d) 1, e) 10, f) 100Vs $^{-1}$. Reproduced with permission.[61] Copyright 1981, Springer.

5.2. Wetting Studies of Sodium on β''-Alumina Ceramic

The theoretical research of the wetting behavior of sodium on β''-alumina starts with a discrepancy between the calculated and experimental value of critical current density at β''-alumina failure when Virkar and Miller tried to prove the Richman-Tennenhouse (R-T) model[63] which used to explain the β''-alumina degradation in liquid sodium. They proposed that non-wetted areas of the β''-alumina surface could induce high local current densities, leading to the degradation of β''-alumina.[64] Afterwards they utilized an electrical mechanical analogue to determine intensification and obtained:

$$i_{tip} = i\left[2\left(\frac{C}{r}\right)^{1/2} + 1\right] \quad (4)$$

where i is current density, $2C$ is the diameter of the unwetted area and r is the crack tip radius.[65] The value of i_{tip} increases as the unwetted area expands. Feldman and De Jonghe suggested that the sodium dendrite would grow out of the high current density region more easily.[66] Therefore, from the perspective of optimizing the Na/β''-alumina interface, it is important to study and improve the wettability of sodium on the β''-alumina surface.

For pristine β''-alumina without treatments, Gibson[67] and Viswanathan et al.[68] obtained the similar results which indicated that the wetting of sodium did not occur at temperature below 300 °C. The incomplete wetting behavior conforms to the previous inferences. For years, many researchers tried to explore the cause of the poor wetting and the methods improving the wettability of sodium on the β''-alumina surface. Two factors arising from moisture and impurity in the β''-alumina ceramic such as calcium were proposed to be responsible. Viswanathan and his coworkers, who pretreated the ceramics in dry or humid environment, demonstrated that the presence of moisture played a role in the poor wetting.[68] Moreover, it has been reported by many researchers that the impurity calcium, introduced in the cell by the ceramic powders during synthesizing the β''-alumina electrolyte, caused obvious increase in cell resistance.[69–72] Mobility and accumulation of calcium on the Na/β''-alumina interface were confirmed by Demott et al. in 1981, who achieved the results through tracking radioactive Ca-45.[73] Later, Lehnert and Hartmann observed tha asymmetric resistance behavior occurred in Na/β''-alumina/Na systems even without current flow owing to the formation of a layer of $Ca(OH)_2$ and CaO.[74]

In order to overcome the negative impact of the impurity, the challenges involved as well as the potential solutions would be discussed. Changing the β''-alumina formulation and treating the Na/β''-alumina interface were considered to be effective ways.[15] Bugden and his coworkers found that using an α-alumina precursor containing less calcium impurity was favorable to the

Table 4 Summary of the wettability of liquid sodium on β″-alumina substrates reported in the literatures.

No.	Treatments for β″-alumina	Mesuring temperature	Test methods	Wettability (contact angle)	Ref.
1	None	<300 °C, >350 °C	X-radiography	Unwetted(>90°), wetted(<90°)	[68]
2	None	260 °C	Sessile drop	Unwetted(160°)	[69]
3	Baked at 425 °C in vacuum for 60hs	360 °C	Sessile drop	Fully wetted(0°)	[69]
4	Exposed to 100% relative humidity for 24hs	360 °C	Sessile drop	Incomplete wetted (103°)	[69]
5	Coating Pb or Bi	250 °C	Immersion tests	Wetted	[77,78]
6	Coating an oxide of a transition metal (Fe,Ni,Cu,Mn,Co,Cr,Mo)	250 °C	Immersion tests	Wetted	[78]
7	Coating liquid $NaNH_2$	210 °C	Sessile drop	Fully wetted(0°)	[79]

decrease of the cell resistance.[75] Nevertheless, more researchers focus on the modification of sodium and the β″-alumina surface.

Table 4 summarizes the wettability of liquid sodium on the surface of β″-alumina substrates reported in the literatures. The effect of the surface treatments were investigated by observing the contact angle between a drop of liquid sodium and the surface of a β″-alumina disc in a inert atmosphere. Many materials including metal (such as Pb, Bi), transition metal oxide, and liquid Na^+ ion conductor $NaNH_2$ were employed to coat on the surface to diminish the contact angle.[76–78] On the other hand, it was found that addition of a Ti or Al to sodium as an oxygen getter to minimize the amount of calcium which is oxidized at the Na/β″-alumina interface, reduced significantly the rate of resistance increase.[73,79] Although these treatments have been proved to be effective, explanation of the mechanism is questionable till now. For example, coating the ceramic surface with a layer of lead greatly improved the wettability of the surface for sodium.[76] It was proposed that the coatings provided an increased surface area to lessen the interference of calcium oxide. For this reason, porous materials are suggested to be a more suitable candidate, which has not been verified. Therefore, the new coating materials and mechanism need to be developed to avoid hazardous substances and enlarge the understanding. Recently, porous carbon films (PCFs) with tunable pore structure have been fabricated by our group to modify the β″-alumina electrolyte surface through a low-cost and direct wet chemistry method followed by a calcination process, which is displayed in **Figure 14**a. As seen in Figure 14b, the porous carbon films were demonstrated to largely improve the wettability of the β″-alumina ceramics by molten sodium at 300 °C. Na/β″-alumina/Na cells were assembled to investigate the interfacial properties between sodium and the β″-alumina electrolyte. The polarization potentials of the cells with and without the PCF coating were measured as a function of the current density, as shown in Figure 14c. The results obtained at 350 °C revealed that the polarization behavior of the cell was improved by the addition of the porous coating.

5.3. Sodium Capillary Wicks

Generally, a traditional sodium anode of NAS battery achieved good contact between sodium and β″-alumina electrolyte by means of three methods: feeding sodium by gravity from a top reservoir, wicking sodium to the β″-alumina surface and forcing sodium from a reservoir by gas pressure. It is noteworthy to emphasize the featured advantages of eliminating the sodium reservoir and using capillary wicks as follows: (1) cost reduction, (2) simplifying sealing process, (3) increasing utilization rate of sodium, (4) improving security of cell on account of restricting the path for sodium, and (5) facilitating a more compact cell design which is more suitable to large capacity energy storage.

As a sodium wick material, several requirements should be satisfied: (1) fully wetted by sodium at the sodium filling temperature, (2) not reacting with liquid sodium, (3) cheap, light and easily incorporated into a cell, (4) not reacting exothermally with sulfur, (5) not releasing gas during warm-up of the cell.

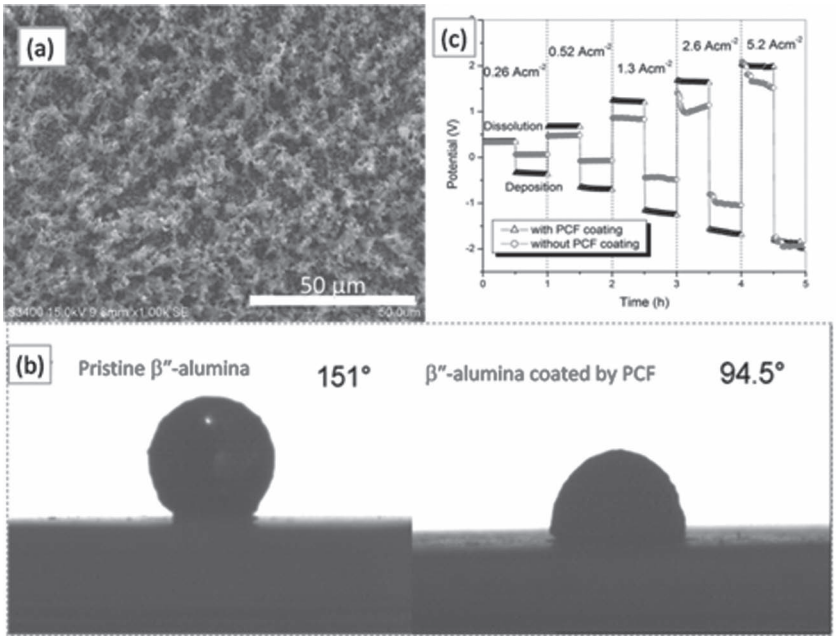

Figure 14. (a) SEM images of the surface of the typical porous carbon film. (b) Optical micrographs of the static sodium drop on β″-alumina with and without the porous carbon coating at 300 °C in argon atmosphere. (c) Constant current polarization curves in Na/β″-alumina/Na cell with and without the porous carbon coating at 350 °C.

Table 5 Summary of the wetting behavior of liquid sodium on various metals and non-metals.

Material	Measuring temperature	Test methods	Wettability (contact angle)	Ref.
Ni, Co, Fe, Mo, W, V, Ti, Zr, Cr	Below 200 °C	Vertical plate	Wetted	[81,82]
Ni, Fe	250 °C	/	Wetted (30°)	[83]
Cr	Below 280 °C, 350 °C	Sessile drop	Unwetted (150°), wetted (75°)	[84]
Fe	Below 330 °C, 350 °C	Sessile drop	Unwetted (120°), wetted (60°)	[84]
Mo	Below 380 °C, 400 °C	Sessile drop	Unwetted (140°), wetted (90°)	[84]
Ni	Below 330 °C, 400 °C	Sessile drop	Unwetted (150°), wetted (75°)	[84]
Al_2O_3, ZrO_2, Y_2O_3, MgO	Below 400 °C	/	Unwetted	[85]

A brief summary of the wetting behavior of liquid sodium on various metals and non-metals is given in **Table 5**. In general, metals are more readily wetted than non-metals, may due to the relative large surface tension of metal,[85] thus metal has the best chance of complete wetting metallic sodium.[86] Metal (such as iron and nickel) shims, gauzes and foams were accordingly common to act as sodium wicks. However, these thin metal wicks could easily be corroded by the molten sulfur and sodium polysulfides produced in the failure reaction, which should be overcome when relying completely on metal wicks to limit the quantity of available sodium.[87] In addition, porous metals and powders are another alternative wicks, especially for vertically operated cells. Knoedler et al. investigated the electrochemical behavior of an sodium electrode containing porous stainless steel felt.[88] They suggested that the optimum pore size was 80 μm with an optimum porosity of approximate 90%. For porous wicks, a close contact between β″-alumina and the porous felts was an issue that was noticeable. Thin porous coatings of nickel and aluminum on a β″-alumina tube prepared by flame spraying or plasma spraying have been patented in 1978,[89] but the synthetic methods were too expensively for further application. Hence, fabrication of large-scale porous metal coatings with controllable surface morphology, porosity, and thickness on the β″-alumina surface is still a great challenge so far. Very recently, novel porous Ni@C coatings on β″-alumina surfaces have been prepared by our group. SEM images in **Figure 15**a shows the Ni@C coating possesses a net-like structure that contained the pores with diameter of ca. 30 μm. Typical cross-sectional (Figure 15b) image clearly displays that the thickness of the as-prepared coating is around 60 μm. In TEM and HRTEM micrographs, it is evident that the Ni nano- or micro-particles (dark part) are coated with a layer of graphite (pale part) with varying thickness. Furthermore, the corrosion behaviors of the coatings in molten sulfur were investigated to demonstrate their high corrosion resistance against molten sulfur. This porous Ni@C coating on the β″-alumina surface has great potential for the sodium wick in NAS batteries.

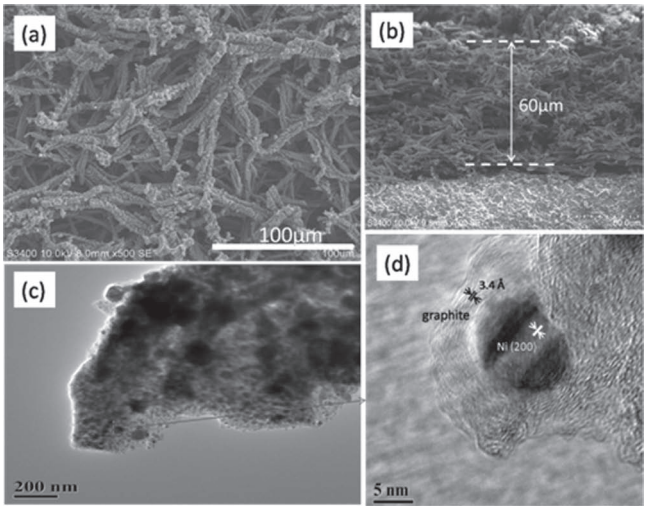

Figure 15. (a) Top-view and (b) cross-sectional SEM images of the typical Ni@C coating. (c) TEM and (d) HRTEM images of the coating.

5.4. Sulfur (Polysulfides)/β″-Alumina Interfaces

We notice that the NAS battery system is not only limited by the performance of the sodium anode. As is well known, sulfur is an electronic insulator, and the electron transfer necessary for electrochemical reaction requires the presence of a porous electronic conductor matrix with high specific surface area in the vicinity of the β″-alumina electrolyte. During discharge, the polysulfide ions are formed on the surface of the conductive matrix near the β″-alumina electrolyte by reaction of sulfur with electrons from the external circuit. During charge, electrons are removed from sodium polysulfide by charge transfer at the surface of the matrix preferentially in the vicinity of the β″-alumina, leaving behind molten sulfur. Since sulfur is nonconductive, when it covers the surface of the porous matrices, charge transfer is forbidden, and the charging process is hindered.[90] With the goal of solving this problem, it is essential to choose a porous inert electronically conducting material with high surface area, which is more readily wetted by polysulfides than sulfur, as the cathode matrix near the solid electrolyte.

Carbon felt (usually graphite felt) is generally believed to be one of the appropriate conductive matrices,[91] and almost universally adopted in cells using β″-alumina electrolyte. Nevertheless, Ludwig reported that graphite was preferentially wet by sulfur as opposed to sodium polysulfide, and he selected porous metal substrate which was coated by an oxide with a thickness of greater than 50 nm.[90] Many other researchers made effects on the improvement of the cathode matrices near the surface of the β″-alumina electrolyte. Carbon foams have been investigated by Sudworth et al. in 1983. They found that

Table 6. The performance of several typical coating materials on Al substrates.[102]

Material	Coating method	Electrical cycling performance
Mo	Flame spray	50 cycles, high resistance
C	PAVD	10 cycles, high resistance
Cr_2C_3	Ion plating	300 cycles, high resistance
Cr_2C_3	Plasma spray	1000 cycles, acceptable performance
$NiCr/Cr_2C_3$	Plasma spray	1000 cycles, acceptable performance
Nb doped TiO_2	Plasma spray	200 cycles, high resistance
Cr_2C_3	Detonation coating	200 cycles, good performance, very expensive
TiO_2/Al_2O_3	Flame spray	10 cycles, high resistance

it is difficult to obtain good contact with the metal current collector.[92] A dispersion of conductive powder in sulfur is another interesting choice for the cathode matrix. South et al. prepared sulfur electrodes from suspensions of carbon black in sulfur, but this method had two disadvantages: low bulk density and high cell resistance at the beginning of discharge.[93] Recently, a mesoporous carbon sphere with the uniform channels has been employed as the conductive matrix in the sulfur cathode for the lithium-sulfur battery.[94] There is still a space to exploit by growing other potential sulfur matrix in the vicinity of the β''-alumina for NAS batteries.

6. Sulfur Electrode Current Collector

As mentioned above, sulfur and the discharged products sodium polysulfide, which are in molten state at the operating temperature of NAS battery (above 300 °C), are extremely corrosive. The corrosion of the positive current collector may lead to loss of capacity, increase of resistance and cycle-life limitations. Therefore, the corrosion of the positive current collector has been considered as one of the major reasons for the failure of NAS battery.[15] The main requirements for the positive current collector include good corrosion resistance, high electrical conductivity, easy fabrication, low weight and low cost. Metals and alloys are either extensively corroded, e.g. Fe, Cu, Ti, Ni and Ni-based alloys,[95] or covered by relatively protective films with low conductivity, e.g. Al, Mo and stainless steel.[96,97] Inorganic compounds such as chromium carbide, titanium carbide or conducting ceramics also have been examined,[98–100] but most of them have certain drawbacks. Composites with an anti-corrosive layer coated on the conducting substrates attracted many researchers' interests and could fulfill the requirements of the positive current collector. **Table 6** summarizes the performance of several typical coating materials on Al substrates.[101] It can be seen that most coated current collectors demonstrate high resistance except plasma sprayed chromium carbides which appear to be satisfactory for several hundred cycles.

We found that perovskite-type oxides, ABO_3, based on rare earth and alkaline earth oxides with 3d transition metal oxides seemed to be promising candidates as the interior coating materials for the sulfur electrode current collectors due to their good electrical conductivity and high stability in both oxidation and reduction environments.[102,103] In our lab, several complex perovskite-type oxides such as $La_{0.8}Sr_{0.2}Co_{0.3}Fe_{0.7}O_{3-\delta}$ (LSCF), $La_{0.8}Sr_{0.2}Co_{0.2}Cr_{0.8}O_{3-\delta}$ (LSCC), $Sr(Co_{0.6}Fe_{0.2}Nb_{0.2})O_{3-\delta}$, etc. were investigated. The corrosion mechanism of these materials in molten sodium tetrasulfide at 350 °C has been studied by electrochemical noise technique, together with potentiodynamic polarization and dip-immersion tests.[104,105] LSCF possessed high electrical conductivity as well as thermal expansion coefficient matching well with the generally used current collector material 316L stainless steel. **Figure 16** a shows the potentiodynamic polarization curves recorded from –30 mV to 30 mV with respect to the corrosion potential (E_{corr}) and the results of the data fitting for LSCF and SS316L exposed to molten sodium tetrasulfide at 350 °C, respectively. The corrosion current density i_{corr} of LSCF obtained from the polarization curve fitting was approximate 10 times smaller than that of SS316L. Figure 16b illustrates the potentiodynamic polarization curves of LSCF and SS316L measured over the wider potential range from –1.60 V to 1.80V versus graphite reference electrode. Compared to SS316L, LSCF showed a rather higher E_{corr} and a relatively smaller passive current, which implied that the passive films formed on the surface of LSCF provided more effective protection against the corrosion attack. However, the corrosion resistance of LSCF against molten sodium tetrasulfide along corrosion time is

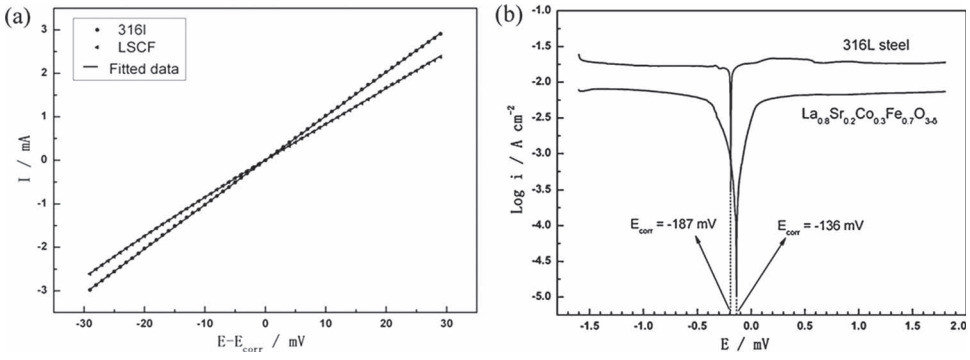

Figure 16. Potentiodynamic polarization curves performed in the potential range of (a) –30 mV to 30 mV and (b) –1.60 V to 1.80 V for the LSCF and SS316L exposed to molten sodium tetrasulfide at 350 °C. Reproduced with permission.[104] Copyright 2010, Elsevier.

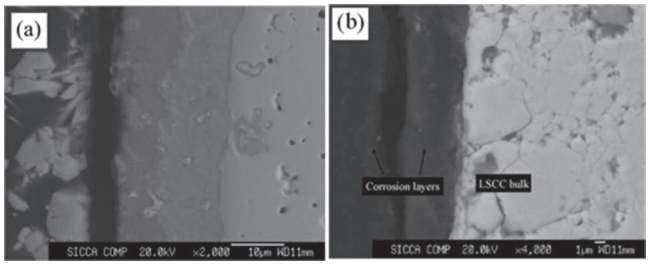

Figure 17. Morphologies of the corrosion surface of (a) LSCF and (b) LSCC immersed in molten sodium tetrasulfide melt for 130 days. Reproduced with permission.[105] Copyright 2011, Elsevier.

limited. The cross section micrograph of LSCF immersed in molten sodium tetrasulfide for 130 days is shown in **Figure 17** a. As seen, the corrosion scale consists of two compact layers. A layer spalled away from the surface with the gaps being filled with epoxy, indicating LSCF degraded to some extent. Besides, $Sr(Co_{0.6}Fe_{0.2}Nb_{0.2})O_{3-\delta}$ and $Sr_{0.8}Ce_{0.2}Ni_{0.4}Cr_{0.6}O_{3-\delta}$ exhibited very low corrosion current density and high corrosion potential, but both displayed cracks after immersing in molten sodium tetrasulfide at 350 °C for several days.

Among those perovskite oxides, LSCC which combines the excellent corrosion resistance with high electrical conductivity turns out to be a promising candidate for the interior coating for the sulfur electrode current collector. The cross-section micrograph of LSCC immersed for 130 days is shown in Figure 17b. Although spallation occurred on the outer surface of the corrosion scale, it didn't influence the evenness and coherence of the corrosion layer. The corrosion rate deduced from immersion test was about 12 μm $year^{-1}$, which was significantly lower than that of aluminum (150 μm $year^{-1}$) and the steel (AISI 446) (90 μm $year^{-1}$).[97] The corrosion current density of LSCC was about 0.08 mA cm^{-2}, approximately two orders of magnitude lower than that of SS316L.

7. Conclusions and Future Outlook

Large scale battery storage technology will play a very important role in the reliable and economic operation of smart electric grids with amounts of renewable power like solar and wind sources. In particular, some countries have set ambitious targets for renewable power sources in the future. It is expected that battery storage technologies can meet the future requirements economically and efficiently. The NAS battery, as one of the most advanced large scale energy storage battery systems, has been widely applied for stationary power storage; it is installed and operating in the energy storage station that is largest in the world (apart from stations using PHS and CAES systems). At present, the NAS battery has occupied nearly 65% market share of large scale energy storage batteries. More and more extensive applications can be expected based on its economic feasibility and optimized performances. As far as the battery technology is concerned, in future there will be significant development in reducing the battery cost and improving their reliability. This article focused on the key materials and the main interfaces in NAS battery, which are among the most important factors determining the performances and cost of the battery.

Since the design of NAS battery is based on many fragile parts involving ceramic electrolyte membrane, glass (ceramic) sealants, and ceramic insulators, for the sake of safety, continuous contributions to improve all the ceramic materials should be made. In addition to the evaluation of NAS cells and module systems, more attention to strict inspection for the ceramic parts has to be paid. New techniques to inspect the parts are meaningful.

Moreover, processes for the most expensive and difficult part β″-alumina ceramic tubes need to be further optimized, which is very helpful to promote the future application of NAS battery and to compete with other large scale battery systems.

It is noticeable that one of the most significant advantages of the present commercial tubular designed NAS battery is its higher energy density in comparison with Li-ion battery and vanadium redox flow battery under development. The enhancement of its power density is very important to widen the application area of the NAS battery. Different designs, for example, planar type, new electrode systems workable at low temperature (100–200 °C) and ambient-temperature sodium (ion) battery are attractive candidates.[8,106–109]

In order to improve the electrochemical performance of NAS battery, particular attention should be paid to the interface behaviors along its inner circuit; optimization of the ceramic electrolyte/electrode interfaces is among the best strategies.

The NAS battery energy storage technology has been commercialized by NGK Insulators Inc. for almost ten years, long period battery maintenance and the recycling cells will be new urgent research topics.

Acknowledgements

The authors appreciate the financial supports from the National Natural Science Foundation of China (No. 50730001) and Chinese Science and Technology Ministry (No. 2007 CB 209700), as well as the research project from the Science and Technology Commission of Shanghai Municipality No. 08DZ2210900. The assistance in experiments and discussion by Mr. Xiaohe Xu, Xiangyu Zhu, Jiadi Cao, Yaming Cui and Miss Yan Lu are highly acknowledged.

Received: February 16, 2012
Revised: March 30, 2012
Published online: May 29, 2012

[1] B. Dunn, H. Kamath, J.–M. Tarascon, *Science* **2011**, *928*, 334.
[2] J. T. Kummer, N. Weber, *U.S. Patent* **1968**, *3413150.*
[3] A. Bito, IEEE Power Eng. Soc. General Meeting, San Francisco, CA **2005**.
[4] R. Dufo-Lopez, J. L. Bernal-Agustin, J. A. Dominguez-Navarro, *Energy Policy* **2009**, *37*, 126.
[5] The vendor's perspective on barriers and issues encountered in U.S. development NGK Insulators Ltd. **2009**. Available: http://www.energy.ca.gov/2009_energypolicy/documents/2009-04-02_workshop/presentations/2_2%20NGK-NAS%20-%20Harold%20Gotschall.pdf. (accessed December 2009)
[6] http://www.ngk.co.jp/english/products/power/nas/index.html (accessed May 2012).
[7] http://www.sgcc.com.cn/ztzl/newzndw/sdsf/10/256776.shtml (accessed May 2012).

[8] X. C. Lu, J. P. Lemmon, V. Sprenkle, Z. G. Yang, *JOM-US* **2010**, *62*, 31.
[9] J. L. Sudworth, P. Barrow, W. Dong, B. Dunn, D. C. Farrington, J. Ö. Thomas, *MRS Bull.* **2000**, *25*, 22.
[10] Z. Yang, J. Zhang, M. C. W. Kintner-Meyer, X. Lu, D. Choi, J. P. Lemmon, J. Liu, *Chem. Rev.* **2011**, *111*, 3577.
[11] T. Oshima, M. Kajita, A. Okuno, *Int. J. Appl. Ceram. Technol.* **2004**, *1*, 269.
[12] G. J. May, S. R. Tan, *Electrochim. Acta.* **1979**, *24*, 755.
[13] A. V. Virkar, G. R. Miller, R. S. Gordon, *J. Am. Ceram. Soc.* **1978**, *61*, 250.
[14] G. E. Youngblood, G. R. Miller, R. S. Gordon, *J. Am. Ceram. Soc.* **1978**, *61*, 86.
[15] J. L. Sudworth, A. R. Tilley, *The Sodium Sulphur Battery*, Chapman and Hall Ltd., New York **1985**.
[16] Y. Sakka, A. Honda, T. S. Suzuki, Y. Moriyoshi, *Solid State Ionics* **2004**, *172*, 341.
[17] X. C. Lu, G. G. Xia, J. P. Lemmon, Z. G. Yang, *J. Power Sources* **2010**, *195*, 2431.
[18] T. Takahashi, K. Kuwabara, *J. Appl. Electrochem.* **1980**, *10*, 291.
[19] A. Pekarsky, P.S. Nicholson, *Mater. Res. Bull.* **1980**, *15*, 1517.
[20] J. Lin, Z. Y. Wen, X. Y. Wang, S. F. Song, Y. Liu, *J. Solid State Electrochem.* **2010**, *14*, 1821.
[21] A. Vanzyl, M. M. Thackeray, G. K. Duncan, A. I. Kingon, R. O. Heckroodt, *Mater. Res. Bull.* **1993**, *28*, 145.
[22] A. vanZyl, *Solid State Ionics* **1996**, *86–88*, 883.
[23] M. Zaharescu, C. Parlog, V. Stancovschi, D. Crisan, A. Braileanu, T. Surdeanu, *Solid State Ionics* **1985**, *15*, 55.
[24] V. Jayaraman, T. Gnanasekaran, G. Periaswami, *Mater. Lett.* **1997**, *30*, 157.
[25] K. G. Chen, Z. X. Lin, Z. Z. Fan, X. H. Xu, Z. Y. Wen, B. Q. Yu, *J. Inorg. Mater.* **1997**, *12*, 725.
[26] Z. Y. Wen, Z. H. Gu, X. H. Xu, J. D. Cao, F. L. Zhang, Z. X. Lin, *J. Power Sources* **2008**, *184*, 641.
[27] Z. Y. Wen, J. D. Cao, Z. H. Gu, X. H. Xu, F. L. Zhang, Z. X. Lin, *Solid State Ionics* **2008**, *179*, 1697.
[28] F. Y. Cheng, J. Liang, Z. L. Tao, J. Chen, *Adv. Mater.* **2011**, *23*, 1695.
[29] R. W. Powers, *J. Electrochem. Soc.* **1975**, *122*, 482.
[30] G. J. Tennenhouse, R. A. Pett, *Fabrication of Thin Layer Beta-Alumina*, NASA Report **1977**, No. CR-135308.
[31] M. Rivier, A. D. Pelton, *Am. Ceram. Soc. Bull.* **1978**, *57*, 183.
[32] A. V. Virkar, G. J. Tennenhouse, R. S. Gordon, *J. Am. Ceram. Soc.* **1974**, *57*, 508.
[33] A. V. Virkar, R. S. Gordon, *J. Am. Ceram. Soc.* **1977**, *60*, 58.
[34] L. Viswanathan, Y. Ikuma, A. V. Virkar, *J. Mater. Sci.* **1983**, *18*, 109.
[35] S. N. Heavens, *J. Mater. Sci.* **1988**, *23*, 3515.
[36] Y. Sheng, P. Sarkar, P.S. Nicholson, *J. Mater. Sci.* **1988**, *23*, 958.
[37] Z. X. Lin, Z. Y. Wen, Z. H. Gu, in *Solid State Ionic Materials*, (Ed: B. V. R. Chowdari), World Scientific Publishing Co., Singapore **1994**, pp. 185.
[38] S. F. Song, Z. Y. Wen, Q. X. Zhang, Y. Liu, *J. Power Sources* **2010**, *195*, 384.
[39] W. G. Budgen, P. R. Smith, *UK Patent* **1989**, GB2 207 545
[40] Y. Akihiko, T. Tomonori, M. Makoto, EP Patent **1996**, 0 729 923.
[41] D. Park, C. Park, *US Patent* **1981**, 4 268 3 13.
[42] F. M. Stackpool, P.W. Mcmillan, *UK Patent* **1987**, GB2 178 589.
[43] S. F. Song, Z. Y. Wen, Y. Liu, Q. X. Zhang, X. W. Wu, J. C. Zhang, J. D. Han, *Ceram. Int.* **2009**, *35*, 3037.
[44] S. F. Song, Z. Y. Wen, Y. Liu, J. Lin, X. W. Wu, Q. X. Zhang, *J. Solid State Electrochem.* **2010**, *14*, 1735.
[45] S. F. Song, Z. Y. Wen, Y. Liu, X. W. Wu, J. Lin, *J. Non-Cryst. Solids* **2011**, *357*, 3074.
[46] S. F. Song, Z. Y. Wen, Y. Liu, *Mater. Lett.* **2010**, *64*, 1025.
[47] D. Linden, T. B. Reddy, *Handbook of batteries*, 3rd edition, The McGraw-Hill Companies, New York **2002**.
[48] M. A. Storey, UK Patent**1977**, GB 1 472 975.
[49] H. Michitaka, F. Kazuhito, S. Masaki, O. Aklyasu, R. Hideki, *EP patent* **2002**, 1 296 392 A2.
[50] J. L. Sudworth, A. R. Tilley, K. D. South, in *Fast ion transport in solids*, (Eds: W. van Gool), North-Holland, New York **1973**, pp. 581.
[51] D. A. Bradhurst, A. S. Buchanan, *Aust. J. Chem.* **1961**, *14*, 397.
[52] R. D. Armstrong, T. Dickinson, J. Turner, *J. Electroanal. Chem. Interfacial Electrochem.* **1973**, *44*, 157.
[53] R. D. Armstrong, T. Dickinson, P. M. Willis, *J. Electroanal. Chem.* **1974**, *53*, 389.
[54] R. D. Armstrong, R. A. Burnham, *J. Electroanal. Chem.* **1976**, *72*, 257.
[55] N. G. Bukun, V. V. Evtushenko, E. A. Ukshe, *Elektrokhimiya* **1974**, *10*, 677.
[56] N. G. Bukun, E. A. Ukshe, V. V. Evtushenko, *Elektrokhimiya* **1973**, *9*, 406.
[57] G. C. Farrington, *J. Electrochem. Soc.* **1976**, *123*, 591.
[58] G. C. Farrington, *J. Electroanal. Chem.* **1977**, *76*, 165.
[59] N. S. Tkacheva, E. A. Ukshe, L. S. Leonova, *Elektrokhimiya* **1978**, *14*, 1405.
[60] M. Voinov, H. Tannenberger, *Electrochim. Acta* **1974**, *19*, 959.
[61] M. W. Breiter, B. Dunn, *J. Appl. Electrochem.* **1981**, *11*, 685.
[62] M. W. Breiter, B. Dunn, *Electrochim. Acta* **1981**, *26*, 1247.
[63] R. H. Richman, G. J. Tennenhouse, *J. Am. Ceram. Soc.* **1975**, *58*, 63.
[64] A. V. Virkar, G. R. Miller, in *Fast Ion Transport in Solids*, (Eds: P. Vashita, J. N. Mundy, G. K. Shenoy), Elsevier-North Holland, New York **1979**, pp. 87.
[65] A.V. Virkar, L. Viswanathan, D. R. Biswas, *J. Mater. Sci.* **1980**, *15*, 302.
[66] L. A. Feldman, L. C. De Jonghe, *ibid.* **1982**, *17*, 517.
[67] A. Gibson, in *Power Sources*, (Eds: D. H. Collis), Academic Press, London **1977**.
[68] L. Viswanathan, A. V. Virkar, *J. Mater. Sci.* **1982**, *17*, 753.
[69] I. W. Jones, L. J. Miles, *Proc. Br. Ceram. Soc.* **1971**, *19*, 161.
[70] A. Imai, M. Harata, *Jan J. Appl. Phys.* **1972**, *11*, 180.
[71] A. C. Buechele, L. C. De Jonghe, *Am. Ceram. Soc. Bull.* **1979**, *58*, 861.
[72] I. Yasui, R. H. Doremus, *J. Electrochem. Soc.* **1978**, *125*, 1007.
[73] D. S. Demott, M. L. Wright, M. D. Hames, *Extended Abstacts 159th Meeting Electrochemical Society*, Minneapolis, **1981**, Abstract 469.
[74] G. Lehnert, B. Hartmann, *Extended Abstacts 162nd Meeting Electrochemical Society*, Detroit, **1982**, Abstract 335.
[75] W. G. Bugden, P. Barrow, J. H. Duncan, *Solid State Ionics* **1981**, *5*, 275.
[76] M. L. Wright, *US Patent* **1980**, 4 348 468.
[77] P. Barrow, M. L. Wright, *US Patent* **1987**, 4 797 332.
[78] N. Weber, I. W. Jones, International Application published under PCT **1991**, WO 91/06133.
[79] M. L. Wright, M. D. Hames, *UK Patent Application* **1982**, 2 080 608.
[80] C. C. Addison, E. Iberson, J. A. Manning, *J. Chem. Soc.* **1962**, 2699.
[81] C. C. Addison, E. Iberson, R. J. Pulham, *Soc. Chem. Ind. Monograph* **1968**, *28*, 246.
[82] B. Longson, J. Prescott, *Liquid Alkali Metals Conference*, British Nuclear Energy Society, Nottingham, England **1973**, p. 171.
[83] E. N. Hodkin, M. Nicholas, *UKAEA Harwell Report AERE* **1976**, R7406.
[84] E. N. Hodkin, M. Nicholas, *Sci. Ceram.* **1979**, *10*, 395.
[85] R. E. Boni, D. Derge, *Trans. Met. Soc. AIME* **1956**, *206*, 53.
[86] G. Kumar, K. N. Prabhu, *Adv. Colloid Interface Sci.* **2007**, *133*, 61.
[87] J. G. Gibson, A. R. Tilley, *US Patent* **1978**, 4 104 448.
[88] R. Knoedler, W. Baukal, W. H. Kuhn, *J. Electrochem. Soc.* **1977**, *124*, 236.

[89] A. R. Tilley, M. D. Hames, J. L. Sudworth, J. M. Bird, *UK Patent Application* **1978**, 1 511 152.
[90] F. A. Ludwig, *US Patent* **1977**, 4 084 042.
[91] J. T. Kummer, N. Weber, *Proc. SAE Congr.* **1967**, paper 670179.
[92] J. L. Sudworth, A. R. Tilley, in *The Sulfur Electrode*, (Eds: R. P. Tischer), Academic Press, New York and London **1983**.
[93] K. D. South, J. L. Sudworth, *143rd meeting Electrochem. Soc.* Chicago **1973**.
[94] X. Liang, Z. Wen, Y. Liu, H. Zhang, L. Huang, J. Jin, *J. Power Sources* **2011**, *196*, 3655.
[95] B. Hartmann, *J. Power Sources* **1978**, *3*, 227.
[96] K. R. Kinsman, W. L. Winterbottom, *Thin Solid Films* **1981**, *83*, 417.
[97] K.E. Heusler, A. Grzegorzewski, R. Knodler, *J. Electrochem. Soc.* **1993**, *140*, 426.
[98] D.S. Park, D. Chatterji, *Thin Solid Films* **1981**, *83*, 429.
[99] A. P. Brown, *J. Electrochem. Soc.* **1987**, *134*, 1921.
[100] H. S. Wroblowa, R. P. Tischer, G. M. Crosbie, G. J. Tennenhouse, *Corros. Sci.* **1986**, *26*, 193.
[101] A. R. Tilley, M. I. Wright, *Proce. 16th IECEC*, Atlanta, **1981**.
[102] S. P. S. Badwal, *Solid State Ionics* **2001**, *143*, 39.
[103] J. W. Fergus, *Solid State Ionics* **2004**, *171*, 1.
[104] Y. Huang, Z. Y. Wen, J. H. Yang, J. D. Cao, Y. Liu, *Electrochim. Acta.* **2010**, *55*, 8632.
[105] Y. Huang, Z. Y. Wen, J. H. Yang, Y. Liu, *Solid State Ionics* **2011**, *192*, 364.
[106] T. C. Girija, A. V. Virkar, *J. Power Sources* **2008**, *180*, 653.
[107] E. Peled, D. Golodnitsky, H. Mazor, M. Goor, S. Avshalomov, *J. Power Sources* **2011**, *196*, 6835.
[108] R. Alcántara, M. Jaraba, P. Lavela, J. L. Tirado, *Chem. Mater.* **2002**, *14*, 2847.
[109] J. Wang, J. Yang, Y. Nuli, R. Holze, *Electrochem. Commun.* **2007**, *9*, 31.